Heliyon 9 (2023) e19435

Contents lists available at ScienceDirect

Heliyon

journal homepage: www.cell.com/heliyon

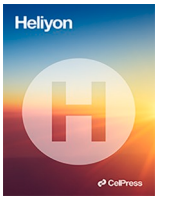

CD3-immunotoxin mediated depletion of T cells in lymphoid tissues of rhesus macaques

Lan Wang [a,b,1], Gajendra W. Suryawanshi [a,b], Shihyoung Kim [d,e,f], Xin Guan [a,b], Aylin C. Bonifacino [g], Mark E. Metzger [g], Robert E. Donahue [g], Sanggu Kim [d,e,f], Irvin S.Y. Chen [a,b,c,*]

[a] Department of Microbiology, Immunology and Molecular Genetics, UCLA, Los Angeles, CA, 90095, USA
[b] Division of Hematology-Oncology, Dept of Medicine, David Geffen School of Medicine, UCLA, Los Angeles, CA, 90095, USA
[c] UCLA AIDS Institute, UCLA, Los Angeles, CA, 90095, USA
[d] Department of Veterinary Biosciences, College of Veterinary Medicine, The Ohio State University, Columbus, OH, 43210, USA
[e] Center for Retrovirus Research, The Ohio State University, Columbus, OH, 43210, USA
[f] Infectious Disease Institute, The Ohio State University, Columbus, OH, 43210, USA
[g] Hematology Branch, National Heart, Lung and Blood Institute, NIH, Rockville, MD, 20850, USA

ARTICLE INFO

Keywords:
CD3 immunotoxin
Tissue staining
Lymphoid tissues
Proliferating CD3 T-cell
Germinal center
T-follicular helper cells

ABSTRACT

Selective T-cell depletion prior to cell or organ transplantation is considered a preconditioning regimen to induce tolerance and immunosuppression. An immunotoxin consisting of a recombinant anti-CD3 antibody conjugated with diphtheria toxin was used to eliminate T-cells. It showed significant T-cell depletion activity in the peripheral blood and lymph nodes in animal models used in previous studies. To date, a comprehensive evaluation of T-cell depletion and CD3 proliferation for all lymphoid tissues has not been conducted. Here, two rhesus macaques were administered A-dmDT390-SCFBdb (CD3-IT) intravenously at 25 μg/kg twice daily for four days. Samples were collected one day prior to and four days post administration. Flow cytometry and immunofluorescence staining were used to evaluate treatment efficiency accurately. Our preliminary results suggest that CD3-IT treatment may induce higher depletion of CD3 and CD4 T-cells in the lymph nodes and spleen, but is ineffective in the colon and thymus. The data showed a better elimination tendency of CD4 T-cells in the B-cell zone relative to the germinal center in the lymph nodes. Further, CD3-IT treatment may lead to a reduction in germinal center T follicular helper CD4 cells in the lymph nodes compared to healthy controls. The number of proliferating CD3 T-cell indicated that repopulation in different lymphoid tissues may occur four days post treatment. Our results provide insights into the differential efficacy of CD3-IT treatment and T-cell proliferation post treatment in different lymphoid tissues. Overall, CD3-IT treatment shows potential efficacy in depleting T-cells in the periphery, lymph nodes, and spleen, making it a

Abbreviations: CD3-IT, CD3-immunotoxin; BM, bone marrow; PB, peripheral blood; LN, lymph nodes; MAC, myeloablative conditioning; RIC, reduced-intensity conditioning; DT, diphtheria toxin; NHP, non-human primate; GC, germinal center; Tfh, T follicular CD4 T cells; ALN, axillary lymph node; SLN, submandibular lymph node; MLN, mesenteric lymph node; IF, immunofluorescent staining; IHC, immunohistochemistry; HC, healthy control; Bcl6, B-cell lymphoma 6.

* Corresponding author. Department of Microbiology, Immunology and Molecular Genetics, University of California, Los Angeles, 615 Charles E Young Drive South, Los Angeles, CA, 90024, USA.
E-mail address: ichen@ucla.edu (I.S.Y. Chen).
[1] Current affiliation: Hearing and Speech Rehabilitation Institute, College of Special Education, Binzhou Medical University, Yantai, China

https://doi.org/10.1016/j.heliyon.2023.e19435
Received 6 December 2022; Received in revised form 11 August 2023; Accepted 22 August 2023
Available online 28 August 2023

viable preconditioning regimen for cell or organ transplantation. Our pilot study provides critical descriptive statistics and can contribute to the design of larger future studies.

1. Introduction

For the treatment of malignant hematological diseases, a preconditioning regimen is conducive in allogeneic and gene-modified autologous cell to allow transplanted cells to efficiently engraft thus reducing the risk of graft rejection [1]. Myeloablative conditioning (MAC) is a type of systemic chemoradiotherapy generally administered to younger patients, whereas reduced-intensity conditioning (RIC), which involves a less toxic dose of alkylating agents and/or radiation, is performed for elderly patients or for those who have conditions which do not allow for MAC [2–5]. Although both methods are efficient for use in the bone marrow (BM) and peripheral blood (PB), adverse events may occur owing to the prolonged time of engraftment, prolonged use of immunosuppressants, or high risk of relapse for RIC [1,6]. In addition, anti-thymocyte globulin (ATG), a polyclonal IgG which targets human thymocytes or T-cells, is also widely used in preconditioning regimens prior to allogeneic stem cell transplantation; however, no clear guidelines exist for optimal ATG dosing [7]. Thus, safer and more targeted preconditioning regimens are being investigated.

Anti-CD3 immunotoxin (CD3-IT) is a fusion protein comprising a targeting moiety, a recombinant anti-CD3 antibody conjugated to a toxic moiety, and a truncated form of diphtheria toxin (DT) [8]. Previous studies have shown that CD3-IT treatment can effectively

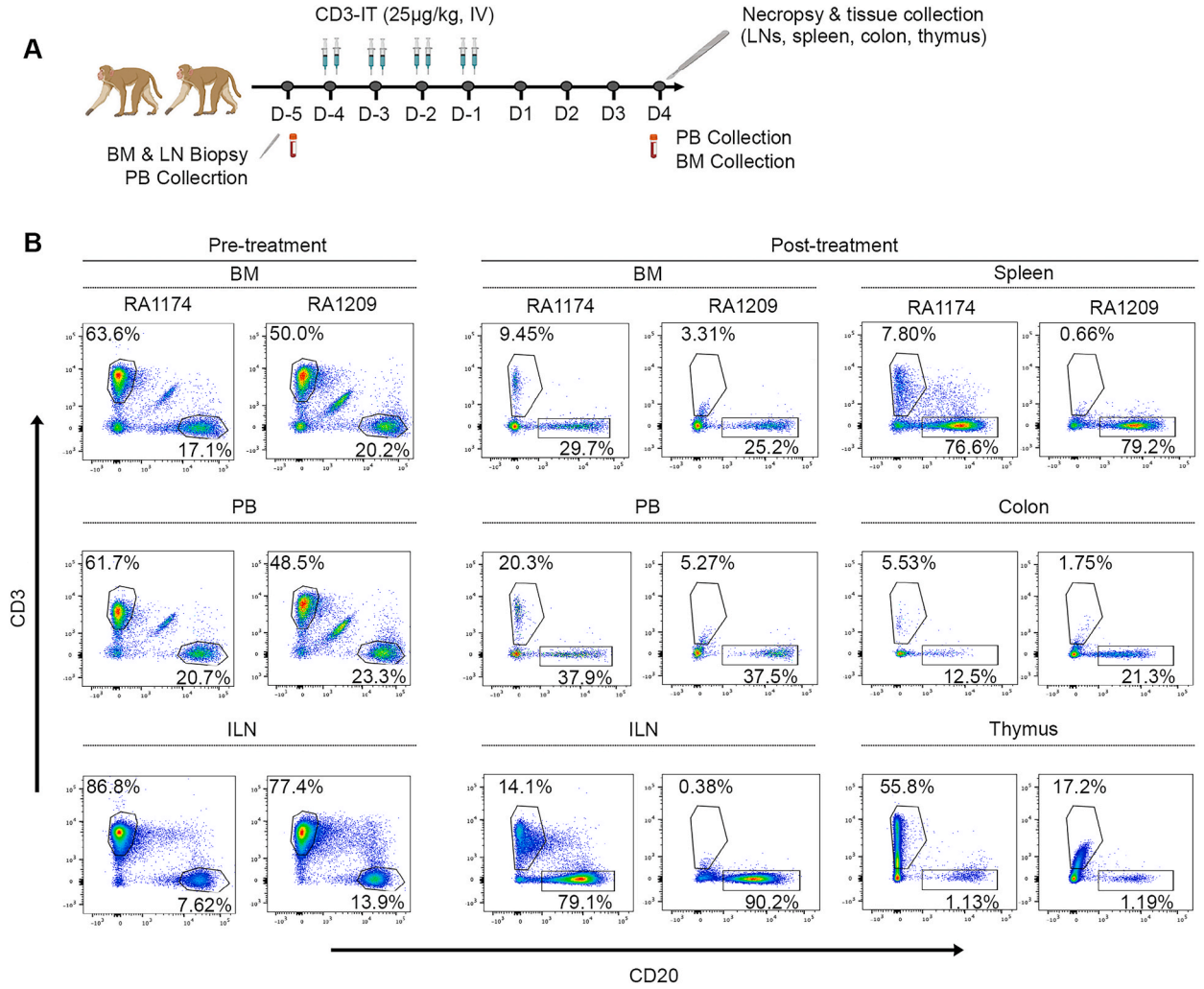

Fig. 1. CD3-IT mediated efficient depletion of CD3 T-cells in multiple organs (A) The schedule of CD3-immunotoxin administration in two rhesus macaques. Bone marrow (BM) and inguinal LN (ILN) biopsies and peripheral blood (PB) samples were collected prior to the treatment; 25 μg/kg of CD3-IT was injected intravenously twice daily for four days; animals were observed for the next four days and then euthanized and necropsied for tissue analysis. (B) Flow cytometry of T-cell (CD3) and B-cell (CD20) subsets prior to (Pre-treatment) and after (Post-treatment) CD3-IT treatment in BM, PB and different lymphoid tissues.

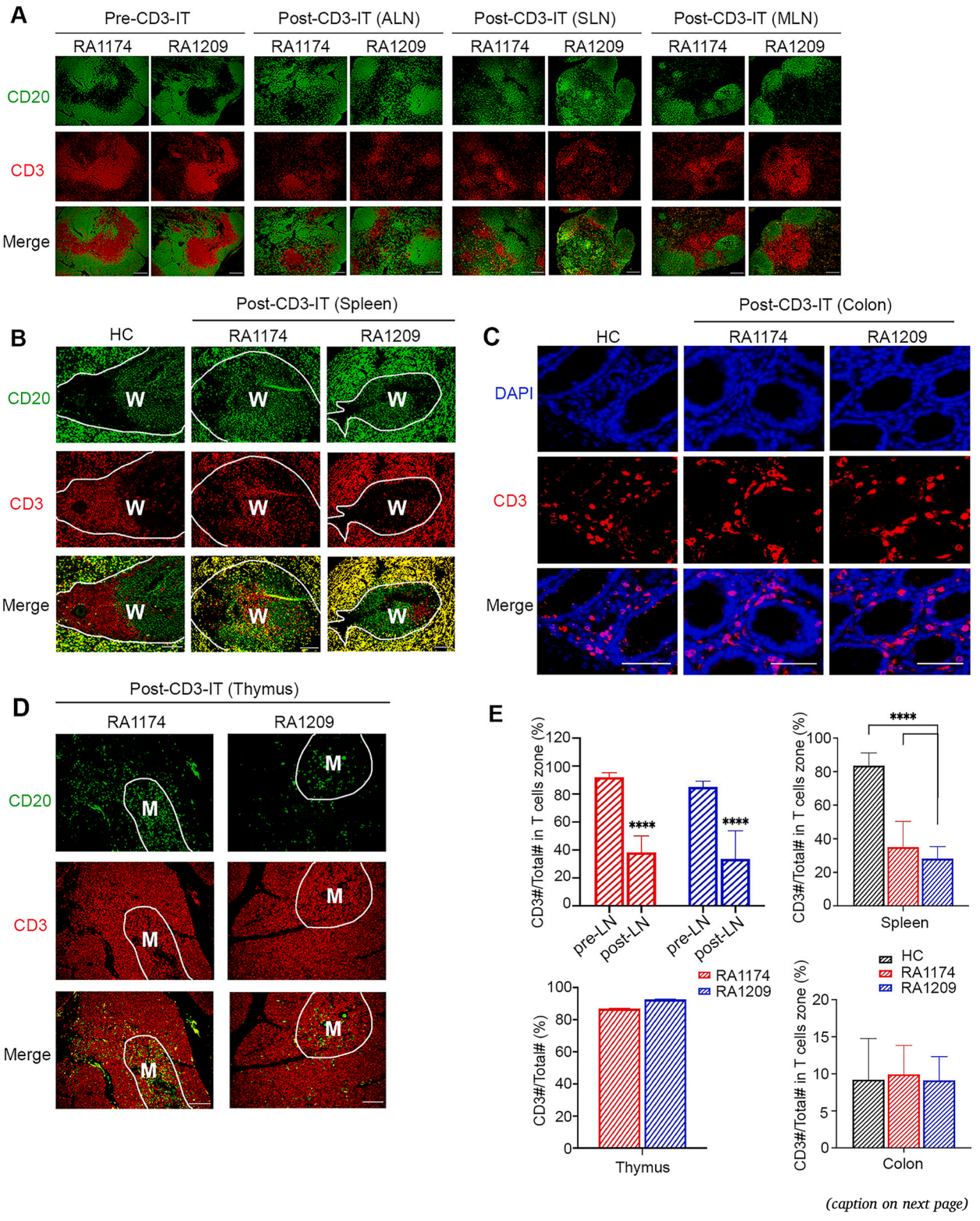

(caption on next page)

Fig. 2. Significant depletion of CD3 T-cells in lymphoid tissues post CD3-IT treatment (A) Co-staining of CD3 and CD20 in the lymph nodes (LNs) pre- and post-CD3-IT treatment. Inguinal LN (ILN) was biopsied and stained as pre-CD3-IT. Axillary, submandibular, and mesenteric LNs (ALNs, SLNs, and MLNs, respectively) were harvested and stained as post-CD3-IT treatment. Scale bar = 200 μm. (B) Staining of CD3 and CD20 in healthy (HC) and CD3-IT-treated spleen. Scale bar = 100 μm; white line-circled area represents the white pulp (W) of spleen. (C) Co-staining of CD3 and CD20 in HC and post treated colon. A 300 × 300 μm region was cropped from each 20× magnification image. Scale bar = 100 μm. (D) CD3 and CD20 staining in thymus post CD3-IT treatment. Scale bar = 100 μm; white line-circled area represents medulla (M), Green represents CD20 B-cells, and red represents CD3 T-cells. (E) CD3 T-cell percentage of different lymphoid tissues is summarized in a histogram (mean ± SD). The mean percentage of CD3 T-cells in the ALNs, SLNs, and MLNs was used for as post-LN. To evaluate the efficacy of CD3 depletion, 107.14 × 107.14 μm of each 20× magnified T-cell zone (n = 6) were selected randomly, and the number of $CD3^+$ cells and total cells in the T-cell zone was calculated by ImageJ software. One-way analysis of variance (ANOVA) with Tukey's multiple comparison was used for statistical analyses of data for the spleen and colon. Two-tailed unpaired *t*-test was used for analyzing efficacy in the LNs, ****$p < 0.0001$.

deplete T-cells in peripheral lymph nodes (LNs) while sparing other immune cells in non-human primates (NHP) [9]. Therefore, CD3-IT can be used to target CD3 molecules as a preconditioning procedure to induce tolerance and immunosuppression prior to cell or organ transplantation [8–10]. CD3-IT application has provided promising results in chronic allograft nephropathy [11] and graft tolerance management studies in both hematopoietic cells [12] and organ transplantation [13–15] in NHP models. However, the efficacy of CD3-IT treatment in other lymphoid tissues, including the spleen, colon, and thymus, remains unclear. Importantly, T-cell recovery from lymphoid tissues after CD3-IT treatment has not been explored. To evaluate its efficacy as a preconditioning regimen, an in-depth understanding of the differential effects of CD3-IT is critical.

In this study, we comprehensively evaluated multiple lymphoid tissues in rhesus macaques four days post CD3-IT treatment. Using a combination of flow cytometry and immunofluorescent (IF) staining, we found that CD3-IT induces more efficient T-cell depletion in the LNs and spleen than in the colon and thymus. Moreover, the treatment is more efficient for eliminating CD4 T-cells in the B-cell zone than in the germinal center (GC) of LNs. Approximately half of the GC T-follicular helper CD4 (Tfh) cells in LNs were depleted. By assessing the number of proliferating CD3 T-cells in different lymphoid tissues, the recovery of T-cells was estimated to be four days post CD3-IT treatment (summarized in the graphical abstract).

2. Results

2.1. CD3-IT treatment efficiently depletes T-cells detected by flow cytometry

The CD3-IT treatment schedule is summarized in Fig. 1A. Two rhesus macaques were used in the present study. PB, BM, and LN biopsies were performed prior to CD3-IT treatment (Day −5; D-5). Animals were injected with CD3-IT intravenously twice daily for 4 days (from D-4 to D-1), PB and BM were collected, and necropsy performed four days post treatment. LNs from different locations, including inguinal LNs (ILNs), axillary (ALNs), submandibular LN (SLNs), mesenteric LN (MLNs), and those from other lymphoid tissues (spleen, thymus, and colon), were harvested during necropsy for T-cell evaluation. Flow cytometry data indicated the efficient depletion of CD3 T-cells in all tissues and in the periphery. As shown in Fig. 1B, high levels of CD3 T-cells were detected in BM, PB, and ILN prior to CD3-IT administration; however, limited T-cell levels were detected at the endpoint for all these samples in both animals. In the BM, the CD3 T-cell count significantly declined from 63.6% to 9.45% for RA1174, and from 50.0% to 3.31% for RA1209, with a mean decline of 50.42% ± 5.28% ($p = 0.0407$). Similar results were observed in PB: CD3 T-cells were decreased from 61.7% to 20.3% in RA1174, and from 48.5% to 5.27% in RA1209, with a mean decrease of 42.32% ± 1.29% ($p = 0.0138$). A significant decline was also observed in the ILN: T-cell count, which decreased from 86.8% to 14.1% in RA1174, and from 77.4% to 0.38% in RA1209, with a mean decrease of 74.86% ± 3.05% ($p = 0.0184$). For other lymphoid tissues, a 7.8% CD3 T-cell count was observed in the spleen of RA1174 and only 0.66% in that of RA1209; further, a 5.53% CD3 T-cell count was detected in the colon of RA1174 and 1.75% in that of RA1209; however, a lower efficiency was observed in the thymus of RA1174 which exhibited 55.8% of remaining CD3 T-cells; however, this was not so in case of RA1209 which exhibited 17.2% of remaining cells (Fig. 1B, post-treatment panel). Overall, the thymus presented the greatest relative resistance to CD3-IT treatment among all the lymphoid organs (55.8% and 17.2% in RA1174 and RA1209, respectively). In addition, compared to RA1174, RA1209 exhibited even better depletion efficacy, with an almost complete depletion of CD3 T-cells (less than 6% cells remained), except for that in the thymus.

2.2. Partial depletion of T-cells after CD3-IT treatment as detected by tissue staining

In addition to flow cytometry, IF tissue staining was used to evaluate the efficacy of CD3-IT treatment in different lymphoid tissues by co-staining with CD20 (indicating the B-cell zone) and CD3 (indicating the T-cell zone) [16,17]. Since we did not collect enough ILN from RA1209 for IF staining, only the ALN, SLN, and MLN were stained and analyzed, and the mean percentage of CD3 T-cells in these three LNs was used to assess the CD3-IT treatment efficacy post treatment. The extent of depletion detected by IF was strikingly different from that detected by flow cytometry. As shown in Fig. 2A, T-cells located at the border of the T-cell and B-cell zones were less sensitive to CD3-IT, but the overall reduction in CD3 T-cells was significant in all three LNs. A higher depletion of CD3 T-cells was observed in ALN and SLN compared to MLN, with fewer cells remaining after CD3-IT treatment. However, the CD3 T-cell counts in these three LNs was unknown prior to treatment, making accurate comparison difficult. The mean percentage of CD3 T-cells in LNs post treatment was 38.4% ± 11.7% in RA1174 and 33.6% ± 20.1% in RA1209, which was much lower than that of the corresponding pre-treatment group (RA1174: 92.0% ± 3.3%; RA1209: 85.0% ± 4.2%) (Fig. 2E upper left). Compared to healthy control (HC: 83.6%

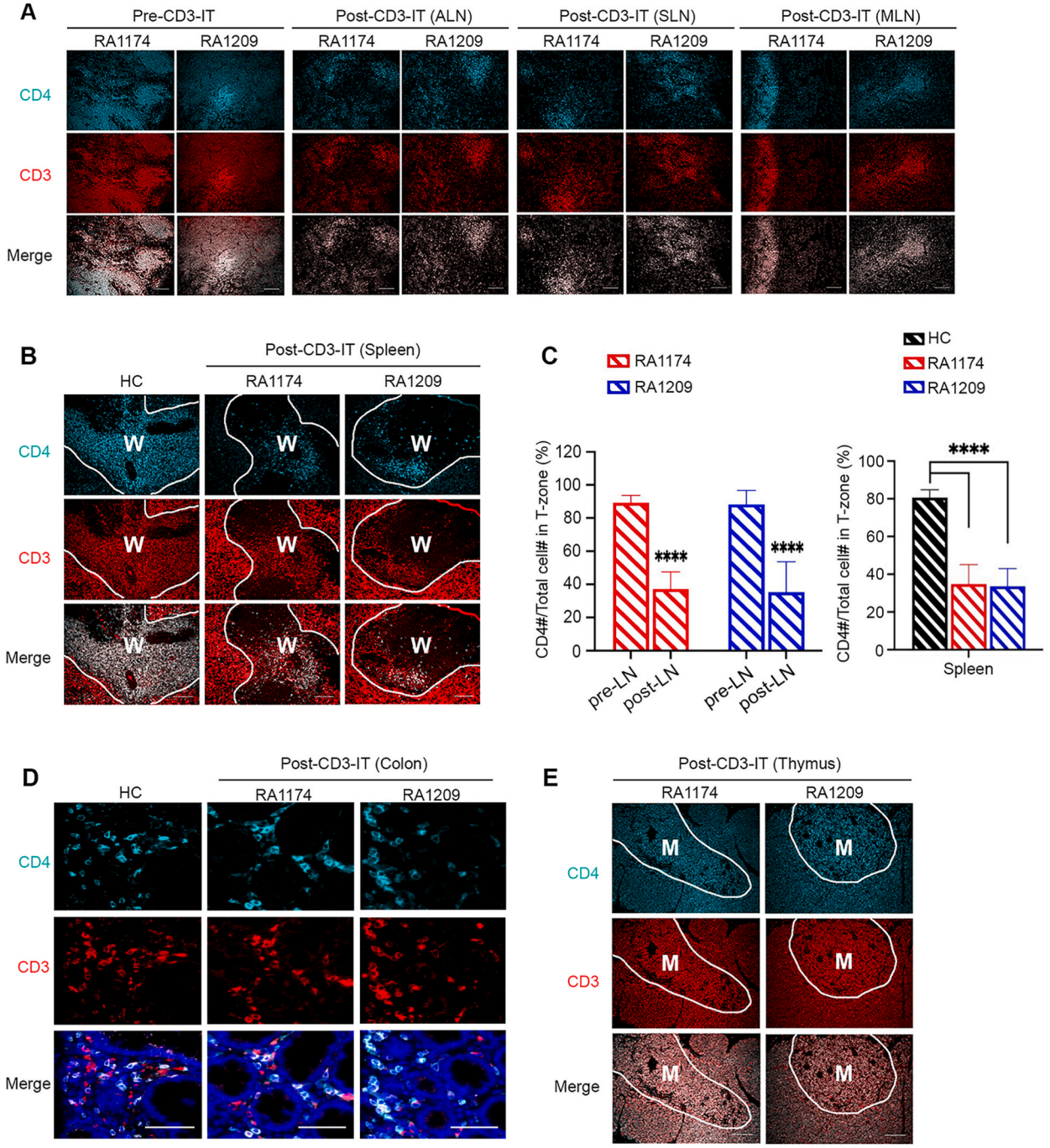

Fig. 3. Efficient depletion of CD4 T-cells post CD3-IT treatment. (A) Co-staining of CD3 and CD4 in the lymph nodes (LNs) pre- and post-CD3-IT treatment. Scale bar = 200 μm. (B) Staining of CD3 and CD4 in healthy (HC)- and CD3-IT-treated spleen. White line-circled area represents the white pulp (W) of spleen, scale bar = 100 μm. (C) Evaluation of CD4 depletion in the LNs and spleen. Inguinal LN (ILN) was used as pre-CD3-IT, the mean percentage of axillary, submandibular, and mesenteric LNs (ALNs, SLNs, and MLNs, respectively) was used as post-CD3-IT. 107.14 × 107.14 μm of each 20× magnified T-cell zone (n = 6) were selected randomly, and the number of $CD4^+$ cells and total cells in the T-cell zone was calculated by ImageJ software. Data is presented as mean ± SD. Two-tailed unpaired *t*-test was used for statistical analyses in the LNs, and one-way analysis of variance (ANOVA) with Tukey's multiple comparison was used for statistical analyses in the spleen, ****$p < 0.0001$. (D) Staining of CD3 and CD4 in HC- and CD3-IT-treated colon. A 300 × 300 μm region was cropped from each 20× magnification image. Scale bar = 100 μm. (E) CD3 and CD4 staining in the thymus post CD3-IT treatment. White line-circled area represents the medulla (M), scale bar = 100 μm, the cyan panel represents CD4 T-cells and the red panel represents CD3 T-cells. Association of CD4 with CD3 T-cells is indicated as white fluorescence in the merged panel.

± 7.5%), 35.1% ± 15.3% and 28.2% ± 7.2% of CD3 T-cells remained in the white pulp (circled area) of the spleen in RA1174 and RA1209, respectively (Fig. 2B & upper right panel of 2E), but no such effect was observed in the colon (Fig. 2C & lower right panel of 2E). Within the thymus, an abundant CD3 T-cell count was identified in the cortex and medulla (circled area) of both animals (87.0% ± 0.12% in RA1174 and 92.7% ± 0.1% in RA1209) (Fig. 2D & lower left panel of 2E). In the absence of healthy or pretreated thymus samples in our study, published data on CD3 T-cell counts in the thymus of age-matched healthy rhesus macaques [18] was used as a reference level for evaluation. In accordance with published control data, CD3 was presented extensively in both the cortex and medulla in our study, which indicates a minimal impact of CD3-IT treatment on the thymus. Taken together, these results show that CD3-IT treatment works efficiently in the LNs and spleen, but is less effective in the colon and ineffective in the thymus.

To further evaluate the impact of CD3-IT treatment on T-cell subtypes, CD3 and CD4 T-cells in the above-mentioned lymphoid tissues were co-stained. The area outside the B-cell follicle was defined as the T-cell zone (the B-cell follicle is not shown in Fig. 3A). As shown in Fig. 2A, the mean percentage of CD4 T-cells in the ALN, SLN, and MLN was used to evaluate CD3-IT treatment efficacy in the LNs after treatment. The presence of CD4 T-cells was highly correlated with that of CD3 T-cells, as shown in the merged panels of Fig. 3. Prior to CD3-IT treatment, the percentage of CD4 T-cells in both recipients was approximately 90% (RA1174: 89.2% ± 4.6%; RA1209: 88.3% ± 8.5%); however, it decreased significantly after CD3-IT treatment (RA1174: 37.1% ± 10.1%; RA1209: 35.3% ± 18.41%) (Fig. 3C, left). Approximately 50% depletion efficacy was observed in the spleen: compared to HC (80.6% ± 4.2%), 34.8% ± 10.3% and 33.6% ± 9.4% of CD4 T-cells were identified in RA1174 and RA1209, respectively (Fig. 3B & C right), but no difference was observed in the colon (Fig. 3D). CD4 T-cells were abundant in the thymus (Fig. 3E).

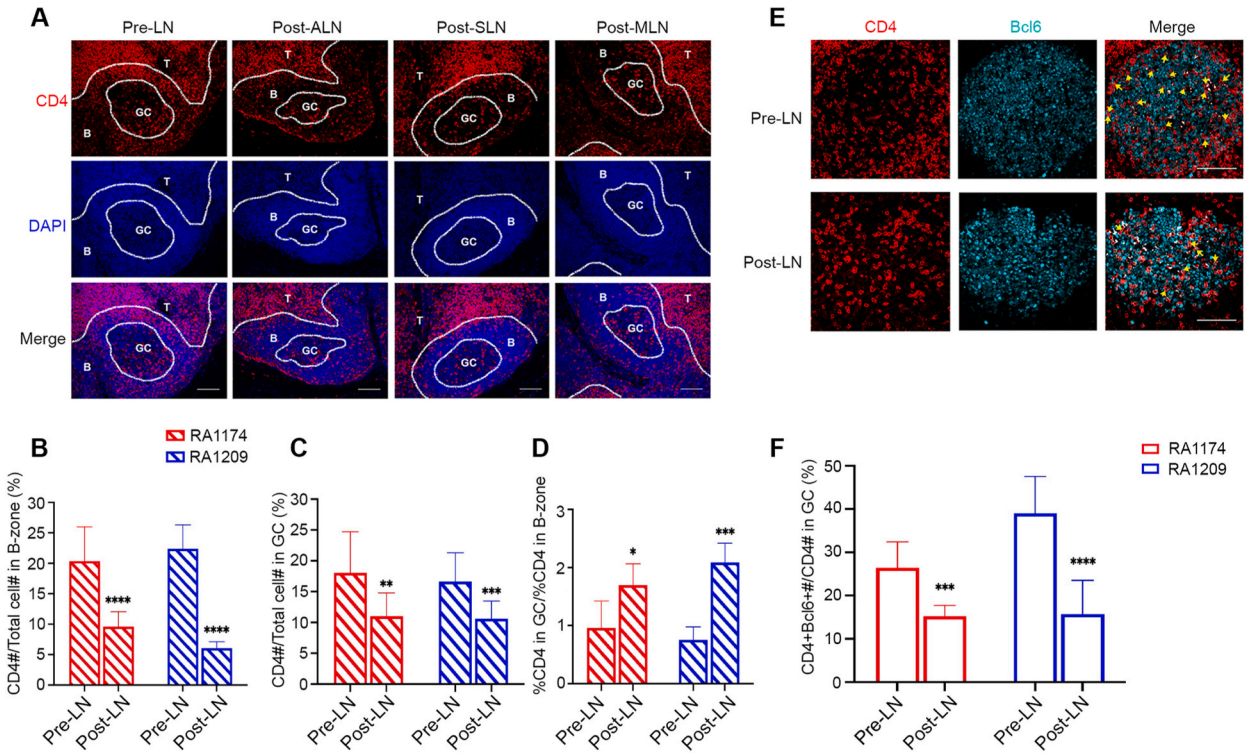

Fig. 4. Lower numbers of CD4 cells in the B-cell zone and GC, and GC Tfh cells in the LNs post CD3-IT treatment (A) Representative images of CD4 T-cells in the B-cell zone (indicated by $CD20^+$ presence; data not shown) and germinal center (GC) (indicated by $Bcl6^+$ cells in $CD20^+$ region, data not shown) of the lymph nodes (LNs) before and after CD3-IT treatment. CD4 T-cells are shown in red and the nuclei are shown in blue. The GC, B-cell zone (B), and T-cell zone (T, the region other than B-cell zone) are indicated accordingly with white lines and letters. Scale bar = 100 μm. Depletion efficacy of CD4 ($CD4^+$ cell count/total cell count) in the B-cell zone (B), and (C) GC, and (D) their changing folds (% CD4 in GC/% CD4 in B-cell zone), are summarized in histograms (mean ± SD), respectively. The mean value of axillary, submandibular, and mesenteric LNs (ALNs, SLNs, and MLNs, respectively) was used as post-LN. 107.14 × 107.14 μm of each 20× magnified T-cell zone (n = 6) were selected randomly, and the number of CD4 T-cells and total cells was calculated by ImageJ software. Two-way analysis of variance (ANOVA) with Tukey's multiple comparison test was used in (B) and (C), and two-tailed unpaired *t*-test was used in (D), *$p < 0.05$, **$p < 0.01$, ***$p < 0.001$, ****$p < 0.0001$. (E) Representative images of GC Tfh cells in the LNs before and after CD3-IT treatment. GC Tfh cells were defined as $CD4^+Bcl6^+$ cells. CD4 is shown in red, Bcl6 is shown in cyan, and representative $CD4^+Bcl6^+$ cells are indicated by yellow arrow. Scale bar = 100 μm. (F) The ratio of $CD4^+Bcl6^+$ cells/$CD4^+$ cells in GC. Data is presented as mean ± SD. The mean value of ALN, SLN, and MLN was used as post-LN. Eight GC-containing follicles were selected randomly, and cell numbers were calculated by Image J. Two-tailed unpaired *t*-test was used for statistical analyses, ***$p < 0.001$, ****$p < 0.0001$.

2.3. More efficient CD4 T-cell depletion in the B-cell zone than in the GC, and reduction of germinal center Tfh cells in the LNs

The number of CD4 T-cells in the B-cell zone (non-GC area) and in the GC area of the LNs was then evaluated prior to and post CD3-IT administration. The B-cell zone was defined as that shown in Fig. 2A (data not shown here), and the region other than the B-cell zone was defined as the T-cell zone. The GC area was defined according to the presence of $Bcl6^+$ cells in the B-cell zone [19]. CD4 T-cell counts decreased significantly in the B-cell zone of all LNs, and the mean percentage of CD4 T-cells in the B-cell zone decreased significantly from 20.7% ± 5.6%–9.6% ± 2.5% ($p < 0.0001$) in RA1174, and from 22.4% ± 3.9%–6.1% to 1.1% ($p < 0.001$) in RA1209 (Fig. 4A and B). In addition, a reduction in CD4 T-cells was also observed in the GC, where cell numbers were decreased significantly from 18.1% ± 6.7%–11.0% ± 3.8% ($p = 0.0048$) in RA1174, and from 16.7% ± 4.6%–10.6% ± 2.9% ($p = 0.002$) in RA1209 (Fig. 4A and C). There was a clear interaction between CD4 T-cells of the B-cell zone and those of the GC (two-way Analysis of Variance (ANOVA), $F_{1,44} = 30.68$, $p < 0.0001$) in RA1209, and CD4 T-cells in the GC were more resistant to CD3-IT treatment compared to those in the B-cell zone (Fig. 4D).

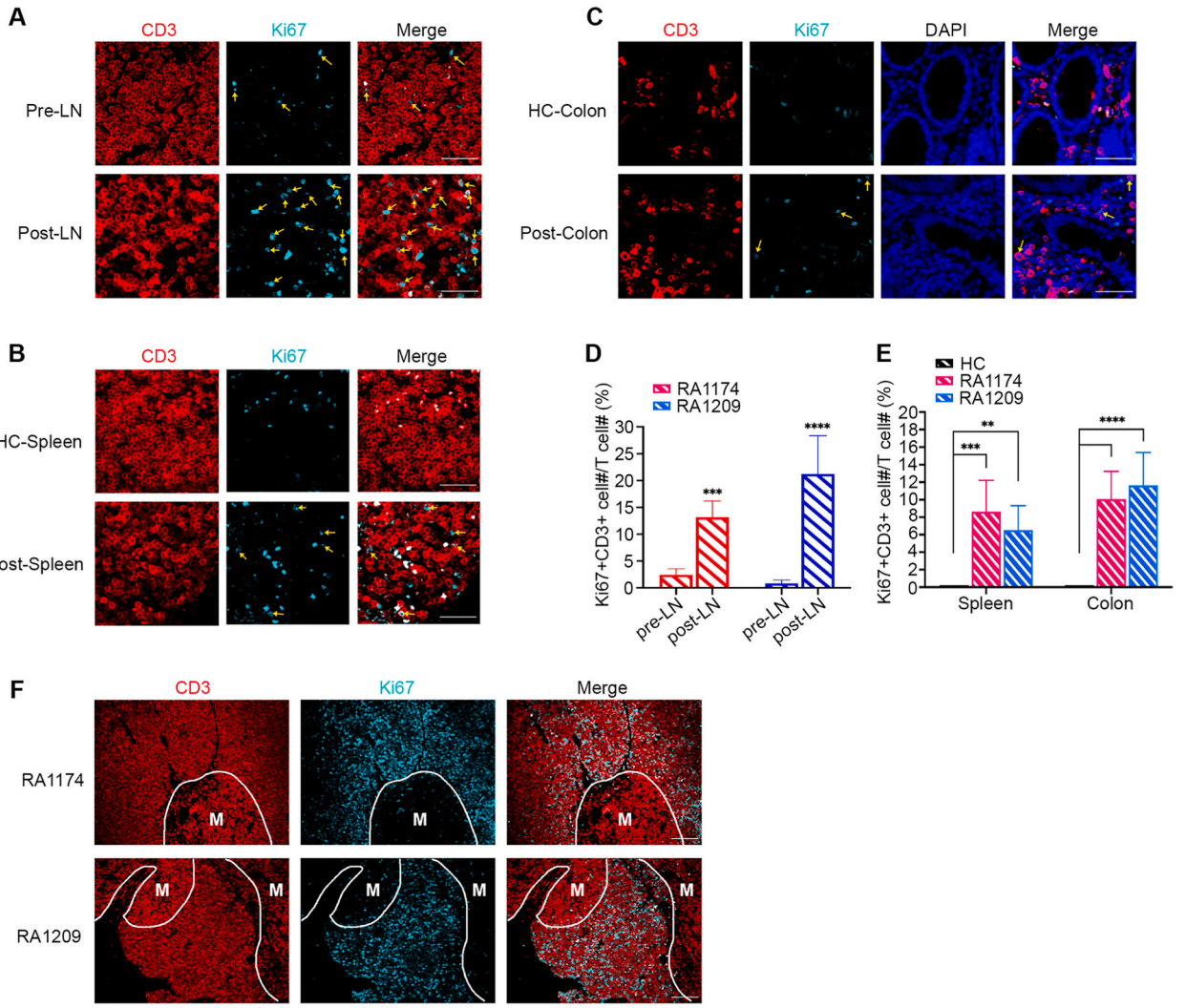

Fig. 5. Higher numbers of proliferating CD3 T-cells post CD3-IT treatment
Representative images of proliferating CD3 T-cells prior to and after CD3-IT administration in the (A) lymph nodes (LNs), (B) healthy (HC) and CD3-IT-treated spleen, and (C) colon. CD3 T-cells are shown in red, and the proliferation marker Ki67 is shown in cyan. $CD3^+Ki67^+$ cells were considered proliferating CD3 T-cells and are indicated by yellow arrows. The nuclei were stained with DAPI and are shown in blue. (D) The ratio of proliferating CD3 T-cells in the LNs (mean ± SD). The mean value of axillary, submandibular, and mesenteric LNs (ALNs, SLNs, and MLNs, respectively) was used as the post-LN. The two-tailed unpaired *t*-test was used for statistical analysis. (E) The ratio of proliferating CD3 T-cells in the spleen (mean ± SD). One-way analysis of variance (ANOVA) with Tukey's multiple comparison test was used for statistical analyses. 107.14 × 107.14 μm of each 20× magnified T-cell zone was selected randomly in (D) and (E) ($n = 6$), and the number of $CD3^+Ki67^+$ cells and total $CD3^+$ T-cells were calculated in T-cell zone using Image J software (**$p < 0.01$, ***$p < 0.001$, ****$p < 0.0001$). (F) CD3 and Ki67 staining in the thymus. The areas labeled 'M' represent the medulla. All images were captured at a magnification of 20×. Scale bar = 100 μm.

GC Tfh cells are specialized providers of T-cells that help B-cells and are essential for GC formation as well as for the generation of long-lived, high-affinity B-cells [20,21]. In this study, the transcription factor B-cell lymphoma 6 (Bcl6) and CD4 were used as indicators to assess the presence of GC Tfh cells ($Bcl6^+CD4^+$). The data showed a significant depletion of Tfh in both animals: the mean percentage of Tfh cells decreased from 26.4% ± 6.0%–15.2% ± 2.5% ($p = 0.0002$) in RA1174, and from 39.0% ± 8.6%–15.7% ± 7.8% ($p < 0.0001$) in RA1209 following CD3-IT treatment (Fig. 4E and F). Taken together, the results indicate that CD3-IT treatment depletes CD4 T-cells more efficiently in the B-cell zone than in the GC and can reduce GC Tfh cells in LNs.

2.4. Increase in the proliferation of CD3 T-cells post CD3-IT treatment

T-cell recovery was evaluated by examining the proliferation of CD3 T-cells in different lymphoid tissues. The cellular proliferation marker Ki67 was co-stained with CD3, and the presence of Ki67 and CD3 double-positive cells ($Ki67^+CD3^+$) indicated the presence of proliferating CD3 T-cells [22]. $Ki67^+CD3^+$ cells were barely detected in the LNs prior to CD3-IT treatment (RA1174: 2.4% ± 1.1%; RA1209: 0.8% ± 0.6%, Fig. 5A & D, Pre-LN), and were not detected in the healthy spleen (Fig. 5B, HC-Spleen) and colon (Fig. 5C, HC-Colon); however, significantly augmented numbers of $Ki67^+CD3^+$ cells were observed four days post T-cell depletion, with a mean increase in LNs (RA1174: 13.2% ± 3.0%, $p = 0.0001$; RA1209: 21.2% ± 7.1%, $p < 0.0001$), as well as in the spleen (RA1174: 8.6% ± 3.6%, $p = 0.0001$; RA1209: 6.5% ± 2.8%, $p = 0.0016$) (Fig. 5B & E) and colon (RA1174: 10.1% ± 3.2%, $p < 0.0001$; RA1209: 11.6% ± 3.8%, $p < 0.0001$) (Fig. 5C & E). In addition, abundant numbers of $Ki67^+CD3^+$ cells, mainly concentrated in the cortex compared to the medulla, were observed in the thymus, which is consistent with previously published human data, showing a stronger positive signal for Ki67 in the cortex than in the medulla of a healthy thymus [23] (Fig. 5F). Taken together, we observed a higher number of proliferating CD3 T-cells in the LNs, spleen, and colon after CD3-IT administration, along with a higher number of proliferating T-cells in the thymus (detected in the cortex than in the medulla), indicating the rapid recovery of CD3 T-cells after CD3-IT treatment.

3. Discussion

CD3-IT administration is a preconditioning regimen used for multiple clinical applications. Our study revealed the effects of CD3-IT treatment on T-cell depletion in multiple lymphoid organs of rhesus monkeys. Our data showed the effective elimination of both CD4 and total CD3 T-cells in peripheral LNs and spleen following CD3-IT treatment, which is consistent with previously published data [9,12]. However, this treatment showed limited efficacy in the colon and thymus. Following treatment, lower levels of T-cells were detected by flow cytometry in the LNs, spleen, and thymus four days post CD3-IT treatment. Interestingly, tissue staining revealed a differential impact of CD3-IT treatment on different lymphoid tissues: T-cells were observed at higher levels, ranging from approximately 30% in the LNs to approximately 40% in the spleen; virtually no depletion (approximately 90% residual) was observed in the thymus, which explains why a thymic irradiation or additional monoclonal antibody injection is included in allograft transplantation protocol in some cases [24–26]. We postulate that flow cytometry detects T-cells that are more similar to their circulating counterparts, which are easily acquired during the cell isolation, whereas tissue staining can detect residual T-cells that are less accessible. Different stromal and fibroblastic reticular cells within the lymphoid organs constitute their internal architecture. These cells mediate lymphocyte migration by serving as scaffolds, and maintain the microenvironment by secreting chemokines, adhesion molecules, and other mediators [27,28]. Thus, it is possible that T-cells are highly adherent to their microenvironment, making it difficult to detect these by flow cytometry. Another reason might be the dilution effect in large population analysis of cells by flow cytometry versus a more localized analysis made possible by tissue staining. Thus, the combined measurement approach used in our study provides both the peripheral and localized impacts of CD3-IT treatment. Overall, our results indicate that a combination of flow cytometry and tissue staining provides more accurate results for evaluating CD3-IT treatment efficiency in lymphoid tissues.

GCs are organized microstructures within B-cell follicles of lymphoid tissues, where memory B-cell and plasma cells are formed [21]. Only a few distinctive T-cells (such as Tfh) can migrate into the GC to induce its formation and the proliferation and generation of long-lived, high-affinity B-cells [20,21]. Compared to other T-helper cell subsets, specific transcription factors, such as Bcl6, the master regulator of Tfh, are used as markers to distinguish Tfh cells [29,30]. In this study, using CD4 and Bcl6 to identify Tfh cells, we observed that the fraction of $Bcl6^+CD4^+$ Tfh cells in the GC of LNs, four days post CD3-IT treatment, was approximately 50% lower than that of the pre-treated samples. Lymphoid organs are thought to be the reservoirs of HIV infection, in the GC of which viruses can hide during infection [31–33] and the clinical latency asymptomatic phase [34,35]. Partially due to the support of Tfh cells in the GC [36,37], the cessation of antiretroviral therapies leads to virus recovery [38]. Considering that CD3-IT treatment depleted approximately half of the Tfh cells in the LNs in our study, this preconditioning approach in combination with CD4-directed chimeric antigen receptor-T-cell therapy, may provide additional benefit for HIV treatment.

In addition to evaluating the depletion efficiency of the immunotoxin, T-cell recovery should also be evaluated after treatment. Ki67 is a nuclear protein that is strictly associated with cellular proliferation [39], and T-cell recovery can be evaluated by co-staining with Ki67 and CD3. Upregulation of proliferating CD3 T-cells was observed in all lymphoid tissues, despite the depletion of T-cells being marginal in the colon and thymus. The increased number of T-cells in the LNs and the spleen implied that the recovery of T-cells started on (or had already started by) day 4 post CD3-IT administration; however, a higher number of animals and time points should be used in future investigations to precisely evaluate the time frame of CD3 T-cell recovery. A previous study showed that Ki67 was broadly expressed in the thymic cortex of 20 human subjects with athymic lesions of various ages [23]. Consistent with these results, in this study, we observed abundant Ki67 expression in the cortex and limited expression in the medulla. The thymus is the primary site of T-cell lymphopoiesis during the early postnatal life, and the cortex, which contains more lymphocytes than the inner medulla, is the initial site for T-cell differentiation [40]. It is believed that T-cells develop in the cortex, migrate to the medulla, and enter the

circulation via lymphatics or blood vessels of the medulla [41]. In this study, because the administration of CD3-IT treatment had no impact on the thymus, T-cells that continued to develop in the cortex could explain the detection of large numbers of proliferating CD3 T-cells. Another possibility is that the elimination of T-cells in the periphery triggered the thymus to produce more T-cells as a homeostatic response, resulting in an increase in proliferating T-cells in the cortex.

This present study had two limitations. One is the limited number of recipients, as this study was a preliminary test of an ongoing study and we had a limited total number of animals. The other limitation is the lack of side-by-side comparisons between the LNs and different anatomic sites, including the thymus. Both factors limited the statistical inferences and estimations. However, this preliminary study provides critical descriptive insights that will inform the future research.

4. Conclusions

This study showed the effect of CD3-IT treatment on multiple lymphoid tissues; the treatment effectively depleted CD3 T-cells and caused a more significant depletion of CD4 T-cells in the B-cell zone than in the GC. It also reduced the number of GC Tfh cells in the LNs by approximately half. The study also revealed the ongoing recovery of T-cells after preconditioning. Overall, our study provides insights into the impact and effectiveness of CD3-IT treatment and supports its application as a preconditioning regimen for cell or organ transplantation.

5. Materials and methods

5.1. Animal care, ethics statements, and treatment

The two rhesus macaques (6-year-old specific pathogen-free males, ID numbers RA1174 and RA1209) used in this study were kept and maintained according to federal guidelines and policies of the Veterinary Research Program of the National Institutes of Health, and the protocols (protocol H-0136R3) were approved by the Animal Care and Use Committee of the National Heart, Lung, and Blood Institute. Recipients were received CD3-IT (A-dmDT390-SCFBdb, C207, NIH Nonhuman Primate Reagent Resource, Cat# PR-0307, RRID: AB2819336) intravenously twice daily for four days at 25 μg/kg [42] over 30 s followed by a 10 ml phosphate buffer saline (PBS) flush [12]. BM and ILN biopsies as well as PB collection was performed prior to the CD3-IT administration, and necropsy was conducted four days post CD3-IT treatment.

5.2. Tissue collection, processing, and flow cytometry

All antibodies used for flow cytometry were purchased from BD Biosciences. PB and BM were collected before necropsy, stored on ice, and processed immediately after collection. Briefly, cells were lysed with ACK RBC lysis buffer (ThermoFisher Scientific), washed with cold 1 × PBS twice, and suspended in staining buffer after cell counting. All lymphoid tissues were collected post perfusion during necropsy. Tissue storage and lymphocyte isolation were performed as previously described [43]. Briefly, tissues were maintained in R10 medium on ice until processing. LNs from different locations, including ALNs, SLNs, MLNs, and ILNs were harvested and split in half: one half was used for flow cytometry and the other was fixed in 10% neutral buffered formalin for paraffin-embedded IF staining. The LNs and spleen were chopped with scissors and placed in sterile petri dishes containing R10 medium and 100 μl of 5 mg/ml DNase1 (Sigma) and then transferred into a 70 μm strainer, meshed with a syringe plunger, collected, and suspended in 200 μl R10 medium. For the thymus and colon, first the fat was removed and then the organs were chopped into small pieces. These were then placed in urine cups supplied with R10 medium, DNase1, and 1 mg/ml of Liberase TM (Roche). Tissue fragments were incubated at 37 °C with rotator for 30 min (thymus) or 60 min (colon). These were then transferred into 70 μm strainers and processed in the same manner as that for the LNs and spleen. The isolated cells were incubated with APC-Cy7 mouse anti-human CD3 (clone sp34-2) and PeCy5 mouse anti-human CD20 (clone 2H7) at 4 °C for 30 min in the dark. Cells were washed twice with staining buffer, fixed with FIX buffer, and analyzed using a BD LSRFortessa™ cell analyzer (BD Bioscience, Inc.). Forward versus side scatter (FSC vs SSC) gating was used to identify cells of interest and to exclude debris, and forward scatter height (FSC–H) versus forward scatter area (FSC-A) density plot was used for doublet exclusion during the cell analysis. The FlowJo software version 10.4 (FlowJo, LLC) was used for further analysis. The. Unstained cells and the single-stained cells, in which only the most positive (brightest) of the positive cells was used, to calculate the compensation.

5.3. Immunofluorescent staining

The tissues were collected and fixed in 10% neutral-buffered formalin (ThermoFisher Scientific). Post paraffin-embedding, ten sections (4 μm thickness) of each sample were cut serially. Staining was performed according to the protocol published on Abcam website (www.abcam.com/protocols/immunocytochemistry-immunofluorescence-protocol). Briefly, the slides were deparaffinized twice in xylene for 20 min and rehydrated in an ethanol gradient. Sodium citrate (Vector Laboratories) was used for the antigen retrieval at 100 °C for 25 min post ddH_2O rinse. The sections were then incubated with BLOXALL endogenous peroxidase and alkaline phosphatase blocking solution (Vector Laboratories) for 10 min at 25 °C, washed with PBST (PBS with Tween-20), and serum blocked at 25 °C for 1 h. Thereafter, the sections were incubated with primary mouse anti-human CD20 (1:200, clone L26, Santa Cruz Biotechnology), rabbit anti-human CD3 (1:100, clone SP7, Invitrogen), mouse anti-human Ki67 (1:500, clone MM1, Leica Biosystems), CD4 (1:200, clone EPR6855, Abcam), and BCL-6 (1:100, clone D8, Santa Cruz), and rabbit anti-human CD8 (1:50, clone SP16,

Invitrogen) in combination or separately overnight at 4 °C. After rinsing with PBST, the slides were incubated with Alexa Fluor 488 conjugated goat anti-mouse IgG2a (1:500, Invitrogen), Rhodamine Red-X (RRX) conjugated donkey anti-rabbit IgG (1:200), Alexa Fluor 647 conjugated goat anti-mouse IgG1 (1:100), Alexa Fluor 647 conjugated goat anti-rabbit IgG (1:500), or Alexa Fluor 680 conjugated goat anti-mouse IgG3a (1:200) (all four from Jackson ImmunoResearch) at 25 °C for 1.5 h. After washing with PBST, the nuclei were counterstained with 4′, 6-Diamidine -2′-phenylindole dihydrochloride (DAPI, Sigma) at 25 °C for 5 min. The slides were then washed with PBST and covered with EverBrite Fluorescence antifade mounting media (VWR). Images were captured using an inverted microscope (DM3000, Leica) and analyzed using Image J software version 2.0 (NIH). In Figs. 2, 3 and 5, six images were captured, and a 107.14 × 107.14 μm region of each image was randomly selected from each $CD3^+$ or $CD4^+$ T-cell image at 20× magnification for analysis (n = 6). Eight GC-containing follicles from each LN were randomly selected as shown in Fig. 4. The number of cells of interest and the total number of cells were calculated using the Image J software.

5.4. Statistical analyses

The results are presented as mean ± standard deviation (SD). Statistical significance was analyzed using GraphPad Prism version 9.2 (La Jolla). A two-tailed paired *t*-test was used to analyze the statistical significance of the flow cytometry data. The results of two-way ANOVA with Tukey's multiple comparison test are shown in Fig. 4B and C. One-way ANOVA with Tukey's multiple comparison test was used to analyze the depletion efficacy in the spleen and colon. A two-tailed unpaired *t*-test was used to analyze the depletion efficacy in the LNs, as shown in Figs. 2, 3 and 4D & 4F, and 5. Statistical significance is presented by p value, * represents $p < 0.05$, ** represents $p < 0.01$, *** represents $p < 0.001$, **** represents $p < 0.0001$.

5.5. Data availability

The data generated from this work are included in this published article, and are available on request to the corresponding author.

Author contribution statement

Lan Wang and Gajendra W. Suryawanshi: Conceived and designed the experiments; Performed the experiments; Analyzed and interpreted the data; Wrote the paper.

Sanggu Kim: Conceived and designed the experiments.

Robert E. Donahue: Conceived and designed the experiments; Contributed reagents, materials, analysis tools or data.

Irvin S.Y. Chen: Conceived and designed the experiments; Contributed reagents, materials, analysis tools or data; Wrote the paper.

Shihyoung Kim, Xin Guan, Aylin C. Bonifacino and Mark E. Metzger: Performed the experiments.

Data availability statement

Data will be made available on request.

Funding

This work was funded by NIH grant 1U19AI149504-01 (IC), supported by the UCLA AIDS Institute, the Intramural Program of the National Heart, Lung, and Blood Institute, and equipment supported by the James B. Pendleton Charitable Trust and the McCarthy Family Foundation.

Declaration of competing interest

The authors declare that they have no known competing financial interests or personal relationships that could have appeared to influence the work reported in this paper.

Acknowledgements

We wish to thank Dr. Cindy Dunbar of the National Heart, Lung, and Blood Institute (NHLBI) for the useful discussions, and Dr. Michael Eckhaus, Dr. Victoria Hoffman, and their team in the NIH Division of Veterinary Resources (DVR) for performing the necropsies. We also wish to thank the veterinarians and technicians of the DVR and NHLBI who assisted in maintaining the monkeys during this study. The Anti-CD3 (C207)-Diphtheria Toxin antibody used in this study was provided by the NIH Nonhuman Primate Reagent Resource (U24 AI126683; P40 OD028116). We thank Dr. Masakazu Kamata at the Department of Microbiology, University of Alabama at Birmingham, for providing slides of healthy spleen and colon.

References

[1] L. Garcia-Perez, L. van Roon, M.W. Schilham, A.C. Lankester, K. Pike-Overzet, F.J.T. Staal, Combining mobilizing agents with busulfan to reduce chemotherapy-based conditioning for hematopoietic stem cell transplantation, Cells 10 (5) (2021), https://doi.org/10.3390/cells10051077.

[2] E. Atilla, P. Ataca Atilla, T. Demirer, A review of myeloablative vs reduced intensity/non-myeloablative regimens in allogeneic hematopoietic stem cell transplantations, Balkan Med. J. 34 (1) (2017) 1–9, https://doi.org/10.4274/balkanmedj.2017.0055.

[3] A. Bacigalupo, K. Ballen, D. Rizzo, S. Giralt, H. Lazarus, V. Ho, J. Apperley, S. Slavin, M. Pasquini, B.M. Sandmaier, J. Barrett, D. Blaise, R. Lowski, M. Horowitz, Defining the intensity of conditioning regimens: working definitions, Biol. Blood Marrow Transplant. 15 (12) (2009) 1628–1633, https://doi.org/10.1016/j.bbmt.2009.07.004.

[4] N. Epperla, K.W. Ahn, M. Khanal, C. Litovich, S. Ahmed, N. Ghosh, T.S. Fenske, M.A. Kharfan-Dabaja, A. Sureda, M. Hamadani, Impact of reduced-intensity conditioning regimens on outcomes in diffuse large B cell lymphoma undergoing allogeneic transplantation, Transplant Cell Ther 27 (1) (2021) 58–66, https://doi.org/10.1016/j.bbmt.2020.09.014.

[5] F. Khimani, M. Dutta, R. Faramand, T. Nishihori, A.P. Perez, E. Dean, M. Nieder, L. Perez, A. Mishra, H. Elmariah, M. Davila, L. Ochoa, M. Alsina, A. Lazaryan, N. Bejanyan, D. Hansen, M. Jain, F. Locke, H. Liu, J. Pidala, B. Shah, R. Mhaskar, Impact of total body irradiation-based myeloablative conditioning regimens in patients with acute lymphoblastic leukemia undergoing allogeneic hematopoietic stem cell transplantation: systematic review and meta-analysis, Transplant Cell Ther 27 (7) (2021) 620 e621–e620 e629, https://doi.org/10.1016/j.jtct.2021.03.026.

[6] I. Sakellari, D. Mallouri, E. Gavriilaki, I. Batsis, M. Kaliou, V. Constantinou, A. Papalexandri, C. Lalayanni, C. Vadikolia, A. Athanasiadou, E. Yannaki, D. Sotiropoulos, C. Smias, A. Anagnostopoulos, Survival advantage and comparable toxicity in reduced-toxicity treosulfan-based versus reduced-intensity busulfan-based conditioning regimen in myelodysplastic syndrome and acute myeloid leukemia patients after allogeneic hematopoietic cell transplantation, Biol. Blood Marrow Transplant. 23 (3) (2017) 445–451, https://doi.org/10.1016/j.bbmt.2016.11.023.

[7] J. Seo, D.Y. Shin, Y. Koh, I. Kim, S.S. Yoon, J. Min Byun, J. Hong, Association between preconditioning absolute lymphocyte count and transplant outcomes in patients undergoing matched unrelated donor allogeneic hematopoietic stem cell transplantation with reduced-intensity conditioning and anti-thymocyte globulin, Ther Adv Hematol 12 (2021), 20406207211063783, https://doi.org/10.1177/20406207211063783.

[8] F. Shafiee, M.G. Aucoin, A. Jahanian-Najafabadi, Targeted diphtheria toxin-based therapy: a review article, Front. Microbiol. 10 (2019) 2340, https://doi.org/10.3389/fmicb.2019.02340.

[9] I. Wamala, A.J. Matar, E. Farkash, Z. Wang, C.A. Huang, D.H. Sachs, Recombinant anti-monkey CD3 immunotoxin depletes peripheral lymph node T lymphocytes more effectively than rabbit anti-thymocyte globulin in naive baboons, Transpl. Immunol. 29 (1–4) (2013) 60–63, https://doi.org/10.1016/j.trim.2013.10.004.

[10] E.K. Page, A.J. Page, J. Kwun, A.C. Gibby, F. Leopardi, J.B. Jenkins, E.A. Strobert, M. Song, R.A. Hennigar, N. Iwakoshi, S.J. Knechtle, Enhanced de novo alloantibody and antibody-mediated injury in rhesus macaques, Am. J. Transplant. 12 (9) (2012) 2395–2405, https://doi.org/10.1111/j.1600-6143.2012.04074.x.

[11] J.R. Torrealba, L.A. Fernandez, T. Kanmaz, T.D. Oberley, J.M. Schultz, K.G. Brunner, D. Peters, J.H. Fechner Jr., Y. Dong, H. Hu, M.M. Hamawy, S.J. Knechtle, Immunotoxin-treated rhesus monkeys: a model for renal allograft chronic rejection, Transplantation 76 (3) (2003) 524–530, https://doi.org/10.1097/01.TP.0000075788.72614.D4.

[12] A.J. Matar, V. Pathiraja, Z. Wang, R. Duran-Struuck, A. Gusha, R. Crepeau, M. Tasaki, D.H. Sachs, C.A. Huang, Effect of pre-existing anti-diphtheria toxin antibodies on T cell depletion levels following diphtheria toxin-based recombinant anti-monkey CD3 immunotoxin treatment, Transpl. Immunol. 27 (1) (2012) 52–54, https://doi.org/10.1016/j.trim.2012.05.003.

[13] D.A. Leonard, J.M. Kurtz, C. Mallard, A. Albritton, R. Duran-Struuck, E.A. Farkash, R. Crepeau, A. Matar, B.M. Horner, M.A. Randolph, D.H. Sachs, C.A. Huang, C.L. Cetrulo Jr., Vascularized composite allograft tolerance across MHC barriers in a large animal model, Am. J. Transplant. 14 (2) (2014) 343–355, https://doi.org/10.1111/ajt.12560.

[14] H. Nishimura, J. Scalea, Z. Wang, A. Shimizu, S. Moran, B. Gillon, D.H. Sachs, K. Yamada, First experience with the use of a recombinant CD3 immunotoxin as induction therapy in pig-to-primate xenotransplantation: the effect of T-cell depletion on outcome, Transplantation 92 (6) (2011) 641–647, https://doi.org/10.1097/TP.0b013e31822b92a5.

[15] M.L. Schwarze, M.T. Menard, Y. Fuchimoto, C.A. Huang, S. Houser, K. Mawulawde, K.S. Allison, D.H. Sachs, J.C. Madsen, Mixed hematopoietic chimerism induces long-term tolerance to cardiac allografts in miniature swine, Ann. Thorac. Surg. 70 (1) (2000) 131–138, https://doi.org/10.1016/s0003-4975(00)01564-2. ; discussion 138-139.

[16] M.R. Neutra, P.A. Kozlowski, Mucosal vaccines: the promise and the challenge, Nat. Rev. Immunol. 6 (2) (2006) 148–158, https://doi.org/10.1038/nri1777.

[17] M. Pino, S. Paganini, C. Deleage, K. Padhan, J.L. Harper, C.T. King, L. Micci, B. Cervasi, J.C. Mudd, K.P. Gill, S.M. Jean, K. Easley, G. Silvestri, J.D. Estes, C. Petrovas, M.M. Lederman, M. Paiardini, Fingolimod retains cytolytic T cells and limits T follicular helper cell infection in lymphoid sites of SIV persistence, PLoS Pathog. 15 (10) (2019), e1008081, https://doi.org/10.1371/journal.ppat.1008081.

[18] Y. Fukazawa, A. Miyake, K. Ibuki, K. Inaba, N. Saito, M. Motohara, R. Horiuchi, A. Himeno, K. Matsuda, M. Matsuyama, H. Takahashi, M. Hayami, T. Igarashi, T. Miura, Small intestine CD4+ T cells are profoundly depleted during acute simian-human immunodeficiency virus infection, regardless of viral pathogenicity, J. Virol. 82 (12) (2008) 6039–6044, https://doi.org/10.1128/JVI.02753-07.

[19] Y. Shaan Lakshmanappa, S.R. Elizaldi, J.W. Roh, B.A. Schmidt, T.D. Carroll, K.D. Weaver, J.C. Smith, A. Verma, J.D. Deere, J. Dutra, M. Stone, S. Franz, R. L. Sammak, K.J. Olstad, J. Rachel Reader, Z.M. Ma, N.K. Nguyen, J. Watanabe, J. Usachenko, R. Immareddy, J.L. Yee, D. Weiskopf, A. Sette, D. Hartigan-O'Connor, S.J. McSorley, J.H. Morrison, N.K. Tran, G. Simmons, M.P. Busch, P.A. Kozlowski, K.K.A. Van Rompay, C.J. Miller, S.S. Iyer, SARS-CoV-2 induces robust germinal center CD4 T follicular helper cell responses in rhesus macaques, Nat. Commun. 12 (1) (2021) 541, https://doi.org/10.1038/s41467-020-20642-x.

[20] S. Crotty, T follicular helper cell differentiation, function, and roles in disease, Immunity 41 (4) (2014) 529–542, https://doi.org/10.1016/j.immuni.2014.10.004.

[21] M. Vaccari, G. Franchini, T cell subsets in the germinal center: lessons from the macaque model, Front. Immunol. 9 (2018) 348, https://doi.org/10.3389/fimmu.2018.00348.

[22] A. Soares, L. Govender, J. Hughes, W. Mavakla, M. de Kock, C. Barnard, B. Pienaar, E. Janse van Rensburg, G. Jacobs, G. Khomba, L. Stone, B. Abel, T.J. Scriba, W.A. Hanekom, Novel application of Ki67 to quantify antigen-specific in vitro lymphoproliferation, J. Immunol. Methods 362 (1–2) (2010) 43–50, https://doi.org/10.1016/j.jim.2010.08.007.

[23] P. Kanavaros, K. Stefanaki, D. Rontogianni, D. Papalazarou, M. Sgantzos, D. Arvanitis, C. Vamvouka, V. Gorgoulis, I. Siatitsas, N.J. Agnantis, M. Bai, Immunohistochemical expression of p53, p21/waf1, rb, p16, cyclin D1, p27, Ki67, cyclin A, cyclin B1, bcl2, bax and bak proteins and apoptotic index in normal thymus, Histol. Histopathol. 16 (4) (2001) 1005–1012, https://doi.org/10.14670/HH-16.1005.

[24] Z.L. Gleit, Y. Fuchimoto, K. Yamada, E. Melendy, R. Scheier-Dolberg, L. Monajati, R.C. Coburn, D.M. Neville Jr., D.H. Sachs, C.A. Huang, Variable relationship between chimerism and tolerance after hematopoietic cell transplantation without myelosuppressive conditioning, Transplantation 74 (11) (2002) 1535–1544, https://doi.org/10.1097/00007890-200212150-00010.

[25] K.W. Lee, J.B. Park, H. Park, Y. Kwon, J.S. Lee, K.S. Kim, Y.J. Chung, J.S. Rhu, S. Choi, G.Y. Kwon, H.J. Kim, E.S. Kang, C.W. Jung, E.C. Shin, T. Kawai, S.J. Kim, J.W. Joh, Inducing transient mixed chimerism for allograft survival without maintenance immunosuppression with combined kidney and bone marrow transplantation: protocol optimization, Transplantation 104 (7) (2020) 1472–1482, https://doi.org/10.1097/TP.0000000000003006.

[26] M.Y. Mapara, M. Pelot, G. Zhao, K. Swenson, D. Pearson, M. Sykes, Induction of stable long-term mixed hematopoietic chimerism following nonmyeloablative conditioning with T cell-depleting antibodies, cyclophosphamide, and thymic irradiation leads to donor-specific in vitro and in vivo tolerance, Biol. Blood Marrow Transplant. 7 (12) (2001) 646–655, https://doi.org/10.1053/bbmt.2001.v7.pm11787527.

[27] N. Eckert, M. Permanyer, K. Yu, K. Werth, R. Forster, Chemokines and other mediators in the development and functional organization of lymph nodes, Immunol. Rev. 289 (1) (2019) 62–83, https://doi.org/10.1111/imr.12746.

[28] K. Knoblich, S. Cruz Migoni, S.M. Siew, E. Jinks, B. Kaul, H.C. Jeffery, A.T. Baker, M. Suliman, K. Vrzalikova, H. Mehenna, P.G. Murray, F. Barone, Y.H. Oo, P. N. Newsome, G. Hirschfield, D. Kelly, S.P. Lee, B. Parekkadan, S.J. Turley, A.L. Fletcher, The human lymph node microenvironment unilaterally regulates T-cell activation and differentiation, PLoS Biol. 16 (9) (2018), e2005046, https://doi.org/10.1371/journal.pbio.2005046.

[29] S. Crotty, Follicular helper CD4 T cells (TFH), Annu. Rev. Immunol. 29 (2011) 621–663, https://doi.org/10.1146/annurev-immunol-031210-101400.

[30] R.I. Nurieva, Y. Chung, G.J. Martinez, X.O. Yang, S. Tanaka, T.D. Matskevitch, Y.H. Wang, C. Dong, Bcl6 mediates the development of T follicular helper cells, Science 325 (5943) (2009) 1001–1005, https://doi.org/10.1126/science.1176676.
[31] P. Biberfeld, A. Ost, A. Porwit, B. Sandstedt, G. Pallesen, B. Bottiger, L. Morfelt-Mansson, G. Biberfeld, Histopathology and immunohistology of HTLV-III/LAV related lymphadenopathy and AIDS, Acta Pathol Microbiol Immunol Scand A 95 (1) (1987) 47–65, https://doi.org/10.1111/j.1699-0463.1987.tb00009_95a.x.
[32] C.H. Fox, K. Tenner-Racz, P. Racz, A. Firpo, P.A. Pizzo, A.S. Fauci, Lymphoid germinal centers are reservoirs of human immunodeficiency virus type 1 RNA, J. Infect. Dis. 164 (6) (1991) 1051–1057, https://doi.org/10.1093/infdis/164.6.1051.
[33] K. Tenner-Racz, P. Racz, M. Bofill, A. Schulz-Meyer, M. Dietrich, P. Kern, J. Weber, A.J. Pinching, F. Veronese-Dimarzo, M. Popovic, et al., HTLV-III/LAV viral antigens in lymph nodes of homosexual men with persistent generalized lymphadenopathy and AIDS, Am. J. Pathol. 123 (1) (1986) 9–15. https://www.ncbi.nlm.nih.gov/pubmed/3008562.
[34] G. Pantaleo, C. Graziosi, J.F. Demarest, L. Butini, M. Montroni, C.H. Fox, J.M. Orenstein, D.P. Kotler, A.S. Fauci, HIV infection is active and progressive in lymphoid tissue during the clinically latent stage of disease, Nature 362 (6418) (1993) 355–358, https://doi.org/10.1038/362355a0.
[35] M. Piatak Jr., M.S. Saag, L.C. Yang, S.J. Clark, J.C. Kappes, K.C. Luk, B.H. Hahn, G.M. Shaw, J.D. Lifson, High levels of HIV-1 in plasma during all stages of infection determined by competitive PCR, Science 259 (5102) (1993) 1749–1754, https://doi.org/10.1126/science.8096089.
[36] S.L. Kohler, M.N. Pham, J.M. Folkvord, T. Arends, S.M. Miller, B. Miles, A.L. Meditz, M. McCarter, D.N. Levy, E. Connick, Germinal center T follicular helper cells are highly permissive to HIV-1 and alter their phenotype during virus replication, J. Immunol. 196 (6) (2016) 2711–2722, https://doi.org/10.4049/jimmunol.1502174.
[37] J.P. Thornhill, S. Fidler, P. Klenerman, J. Frater, C. Phetsouphanh, The role of CD4+ T follicular helper cells in HIV infection: from the germinal center to the periphery, Front. Immunol. 8 (2017) 46, https://doi.org/10.3389/fimmu.2017.00046.
[38] F. Maldarelli, S. Palmer, M.S. King, A. Wiegand, M.A. Polis, J. Mican, J.A. Kovacs, R.T. Davey, D. Rock-Kress, R. Dewar, S. Liu, J.A. Metcalf, C. Rehm, S.C. Brun, G.J. Hanna, D.J. Kempf, J.M. Coffin, J.W. Mellors, ART suppresses plasma HIV-1 RNA to a stable set point predicted by pretherapy viremia, PLoS Pathog. 3 (4) (2007) e46, https://doi.org/10.1371/journal.ppat.0030046.
[39] T. Scholzen, J. Gerdes, The Ki-67 protein: from the known and the unknown, J. Cell. Physiol. 182 (3) (2000) 311–322, https://doi.org/10.1002/(SICI)1097-4652, 200003)182:3<311::AID-JCP1>3.0.CO;2-9.
[40] M. Nishino, S.K. Ashiku, O.N. Kocher, R.L. Thurer, P.M. Boiselle, H. Hatabu, The thymus: a comprehensive review, Radiographics 26 (2) (2006) 335–348, https://doi.org/10.1148/rg.262045213.
[41] M.A. Weinreich, K.A. Hogquist, Thymic emigration: when and how T cells leave home, J. Immunol. 181 (4) (2008) 2265–2270, https://doi.org/10.4049/jimmunol.181.4.2265.
[42] E.J. Kim, J. Kwun, A.C. Gibby, J.J. Hong, A.B. Farris 3rd, N.N. Iwakoshi, F. Villinger, A.D. Kirk, S.J. Knechtle, Costimulation blockade alters germinal center responses and prevents antibody-mediated rejection, Am. J. Transplant. 14 (1) (2014) 59–69, https://doi.org/10.1111/ajt.12526.
[43] D. Stone, E.J. Kenkel, M.A. Loprieno, M. Tanaka, H.S. De Silva Feelixge, A.J. Kumar, L. Stensland, W.M. Obenza, S. Wangari, C.Y. Ahrens, R.D. Murnane, C. W. Peterson, H.P. Kiem, M.L. Huang, M. Aubert, S.L. Hu, K.R. Jerome, Gene transfer in adeno-associated virus seropositive rhesus macaques following rapamycin treatment and subcutaneous delivery of AAV6, but not retargeted AAV6 vectors, Hum. Gene Ther. 32 (1–2) (2021) 96–112, https://doi.org/10.1089/hum.2020.113.